Jurnal Kejuruteraan 17 (2005) 13-26

# Determination of Enhancement in D-region Electron Density using Solar Flare Model and GOES-7 Measurements

Mardina Abdullah and Ahmad Faizal Mohd. Zain

ABSTRACT

*This investigation elucidates the enhancement of production of electrons in the ionospheric D region by soft solar X-ray flares. A simple solar X-ray flare model is established for the purpose of this study. The in-step variation of calculated enhanced electron densities with measured values of enhanced flux intensities obtained by the GOES-7 X-ray detector is understood quantitatively by the difference of arrival time of the maximum enhanced electron density with the arrival time maximum enhanced flux intensity i.e., the arrival time lag. This is compared with time lag taken from the X-ray flare model under the condition that the enhanced the electron densities are much smaller than electron density in a quiet state. The comparison of theoretical time lag or the response rate shows a good agreement with that obtained by measurements. By using this model, physical quantities such as the decreasing slope coefficient of flare model $\beta(\chi, z)$ are described in detail to identify their effects to enhanced electron densities. Good or poor in-step variation of enhanced electron densities to enhanced flux intensities through their increasing, maximum and decreasing stage is mostly dependent on fundamental physical quantities $\beta(\chi, z)$, by evaluation of the response rate. Time lag, which is inversely proportional to $\beta(\chi, z)$, shows good response. The temporal variation of $\beta(\chi, z)$ is also studied. This result can also be applied to disturbance phenomena that have a similar form.*

*Keywords: flare model, electron densities, soft solar X-ray, flux intensities, GOES-7*

ABSTRAK

*Kajian ini menyelidik peningkatan dalam pengeluaran elektron dalam kawasan D inosfera dengan kehadiran nyala sinar-X lembut suria. Model mudah nyala sinar-X diwujudkan untuk tujuan kajian ini. Variasi langkah antara peningkatan ketumpatan elektron secara kiraan dan nilai ukuran peningkatan keamatan fluks yang diperoleh dari alat pengesan sinar X GOES-7 difahami secara kuantitatif dengan perbezaan masa tiba peningkatan ketumpatan elektron maksimum dengan masa tiba peningkatan keamatan fluks atau susulan masa tiba. Ini dibandingkan dengan susulan masa yang diambil dari model nyala dalam keadaan peningkatan ketumpatan elektron jauh lebih kecil daripada ketumpatan elektron dalam keadaan tidak aktif. Perbandingan susulan masa secara teori atau kadar gerak balas ini menunjukkan persetujuan baik dengan susulan masa yang didapati melalui pengukuran. Dengan menggunakan model ini, kuantiti fizik seperti pengurangan kecerunan pekali model nyala dan $\beta(\chi, z)$ diterangkan dengan lebih*

*terperinci untuk mengenal pasti kesannya terhadap peningkatan ketumpatan elektron. Baik atau buruknya variasi langkah peningkatan ketumpatan elektron terhadap peningkatan keamatan fluks melalui tahap naik, maksimum dan turun amat bergantung kepada kuantiti fizik $\beta(\chi, z)$ dengan menghitung kadar gerak balasnya. Susulan masa ini adalah berkadar songsang dengan $\beta(\chi, z)$. Variasi masa $\beta(\chi, z)$ ini juga telah di kenalpasti. Keputusan kajian ini telah diaplikasikan terhadap fenomena gangguan yang mempunyai ciri yang sama.*

*Kata kunci: model nyala, ketumpatan elektron, sinar-X lembut suria, keamatan fluks, GOES-7*

## INTRODUCTION

Solar flares are among the most energetic explosions in the solar system, which have a direct effect on the Earth's atmosphere. After eight minutes of its occurrence, its intense radiation will travel to Earth resulting the Earth's upper atmosphere to become more ionized and expanded. (Dellinger 1937) described this sudden increase in ionization as Sudden Ionospheric Disturbance (SID), which produces phenomena like short wave fade out (SWF), sudden phase anomaly (SPA) and others. These phenomena occur simultaneously and will disrupt long distance radio wave propagation. These effects indicate an increase of electron concentration in the ionospheric D region, which will increase absorption of electromagnetic wave. From satellite measurements, it is clearly identified that the solar soft X-ray (SSX-ray) enhancement is responsible for the D region SID effects (Ohshio 1978; Rishbeth 1969). Even though the hard X-ray that can be measured by the Yohkoh satellite at present penetrates deeper into the Earth's atmosphere, the distinction between hard and soft X-ray is still not well defined (Bentley & Phillips 1995; Holman & Benedict 1999).

From the stand point of ionosphere and radio propagation, there are a number of terrestrial effects observed which provide information about the flare mechanism. The understanding of this mechanism will be very useful for the prediction and forecasting of ionospheric radio propagation especially for the next maximum solar activity, expected in year 2011. This paper focuses on the identification of the physical quantities that determine the response of enhanced electron density, $\Delta N(\chi, z, t)$ to enhanced flux intensities $\Delta F(\lambda, t)$, using the flare model. The model of enhanced production rate of electron-ion pairs, $\Delta q$, represents the SSX-ray ($\lambda$ = 0.05 nm~0.8 nm) flux intensity that penetrates into the D region, at a height of z = 60 ~ 90 km, to stimulate $\Delta N(\chi, z, t)$ and presents a study of their response. The time lag is expressed by a response rate, $R$ to show the best response of $\Delta N(\chi, z, t)$ to $\Delta F(\lambda, t)$. The time lag obtained from the model has been compared with that taken from observation to justify the model. The dynamic characteristics of the time variation in the height distribution of $\beta(\chi, z)$ is described and used to explain the characteristic of time lag.

# THEORETICAL CONSIDERATION

## A FLARE MODEL

During a solar X-ray flare, the production of electrons is dependent on recombination process and the density during the quiet state. The rate of change of $\Delta N$ with respect to time is given by

$$\frac{d\Delta N}{dt} = \frac{\Delta q}{1+\lambda(z)} - 2\alpha_{eff} N_q \Delta N - \alpha_{eff} \Delta N^2, \quad (1)$$

where,

$\alpha_{eff}$ : effective recombination coefficients,
$N_q$ : electron density during the quiet state,
$\lambda(z)$ : wavelength,
$\Delta q$ : enhanced production rate of electron-ions pairs.

From the previous work, (Abdullah & Zain 2000), Millington, Riccati and Taylor's method were used to solve the above equation. Besides the time lag and electron production ratio, etc, physical quantities such as $\Delta q$, $\lambda(z)$, $\alpha_{eff}$, and $N_q$ in equation (1) also affect the variation of $\Delta N(t)$. However, this cannot be identified using the methods mentioned. Thus, in order to determine the physical mechanisms which really affect the variation of $\Delta N(t)$, an approximation

$$\frac{\Delta N(x,z,t)}{N_q(x,z)} << 1, \quad (2)$$

is used. By considering equation (2), equation (1) can be rewritten as,

$$\frac{d\Delta N}{dt} = \frac{\Delta q}{1+\lambda(z)} - 2\alpha_{eff} N_q \Delta N. \quad (3)$$

For a single wavelength range and for all times, the rate of electron-ion pair production $\Delta q$ ($\chi$, $z$, $t$) is proportional to $\Delta F$ ($\lambda_l \sim \lambda_u$, $t$). This can be expressed by,

$$\Delta q(\chi,z,\lambda_i,\Delta F(\lambda_l \le \lambda \le \lambda_u,t)) = \sum_{i=1}^{m} Y_i(\chi,z,\lambda_i)\frac{\lambda_i}{hc}\Delta F(\lambda_l \le \lambda_i \le \lambda_u,t)\frac{\delta\lambda_i}{\lambda_u - \lambda_l}, \quad (4)$$

where,

$Y(\chi, z, \lambda)$ : local photoionization efficiency,
$\lambda_i$ : wavelength which included in $[\lambda_{lower} \le \lambda \le \lambda_{upper}]$ with $\delta\lambda_i$ divided to m wavelength,
$h$ : Planck's constant (= $6.626 \times 10^{-34}$ J s),
$c$ : light velocity in vacuum (= $2.998 \times 10^{8}$ m $s^{-1}$),
$\Delta F$ : enhanced flux intensity.

Hence $\Delta q(\chi, z, t)$ can be used to express the flare model.

For the model to work, taking into consideration that the approximations, have to satisfy the following conditions.

(i) During the increasing electron-ion pair production phase

$$\Delta q(\chi, z, 0, \leq t \leq t_m) = At^n, \tag{5}$$

where,

$n$ : integer,

$A$ : proportional constant.

(ii) When the electron-ion pair reaches its maximum production rate, then

$$\Delta q(\chi, z, t_m \leq t \leq t_{me}) = \Delta q_m = \text{constant} \tag{6}$$

where,

$$t_{me} - t_m = \tau_m.$$

(iii) After the electron-ion pair reaches its maximum value, it will decrease according to

$$\Delta q(\chi, z, t_m \leq t \leq t_{me}) = \phi_d(\chi, z) e^{-Bt}, \tag{7}$$

where,

$\phi_d$ : proportional constant,

$B$ : decreasing coefficient of $\Delta q$.

Under the condition of equation (2), $\Delta q(\chi, z, 0, \leq t \leq t_m)$ increases proportionally to $t^n$ of time, $t$, and after reaching the maximum period at $\tau_m (= t_{me} - t_m > 0)$, $\Delta q(\chi, z, t_{me} \leq t \leq t_e)$ decreases proportionally to $e^{-Bt}$ to satisfy $\Delta q(t_{me} + t_d) = b\Delta q(t_{me})$. The model is shown in Figure 1.

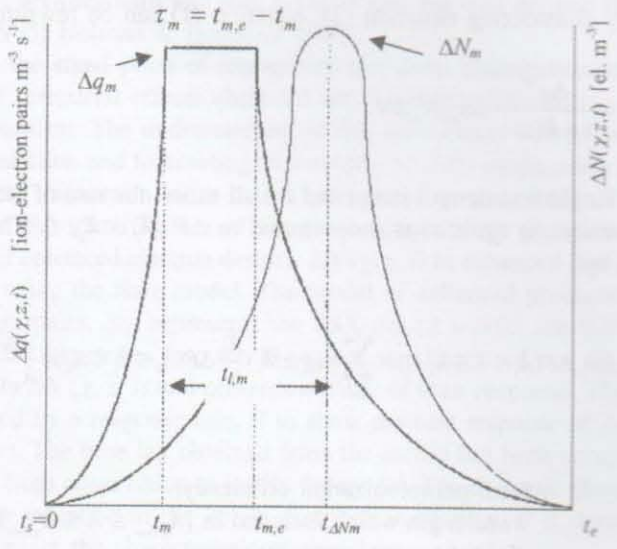


FIGURE 1. Flare model

$\Delta N(\chi, z, t)$ is derived by integrating equation (3) and by using the flare model. The general solution of equation (3) is given by

$$\Delta N = e^{-\beta t}\left\{\int \frac{\Delta q(t)}{\gamma} e^{\beta t} dt + C\right\}, \tag{8}$$

where,

$$\beta(\chi, z) = 2\alpha_{eff}(z) N_q(\chi, z), \tag{9}$$

$$\gamma(z) = 1 + \lambda(z), \tag{10}$$

$C$ = constant.

*Increasing stage of $\Delta N$*

The general solution during the increasing stage is obtained from equation (5) and equation (8) as

$$\Delta N(\chi, z, 0 \le t \le t_m) = \Delta N_\infty \frac{t^n}{t_m^n}\left\{1 + \sum_{i=1}^{n-1}(-1)^i \frac{1}{(\beta t)^i}\frac{n!}{(n-i)!} + (-1)^n \frac{n!}{(\beta t)^n}(1 - e^{-\beta t})\right\}, \tag{11}$$

where,

$$\Delta N_\infty(\chi, z, t) = \frac{\Delta q_m(\chi, z, t)}{\gamma(z)\beta(\chi, z)}, \tag{12}$$

by considering initial conditions, $t_s = 0$, and $\Delta N(t_s) = 0$.

The integer, $n$, is defined by comparing the measured $\Delta F$ during the decreasing stage by substituting $n$ in equation (11) since $\Delta q(\chi, z, t)$ is proportional to $\Delta F(\lambda_l \sim \lambda_u, t)$. Figure 2 representatively shows that $n = 4$ is the nearest to $\Delta F$. By substituting n in equation (11), $\Delta N$ can be rewritten as

$$\Delta N(\chi, z, 0 \le t \le t_m) = \Delta N_\infty \frac{t^4}{t_m^4}\left\{1 - \frac{4}{\beta t} + \frac{12}{\beta^2 t^2} - \frac{24}{\beta^3 t^3} + \frac{24}{\beta^4 t^4}(1 - e^{-\beta t})\right\}. \tag{13}$$

*Maximum stage of $\Delta N$*

$\Delta N$ at maximum stage is obtained from equation (6) and equation (8). Equation (13) is also used when $\Delta N(t_m)$ at the maximum stage is equal to $\Delta N(t_m)$ during the increasing stage. $\Delta N(\chi, z, t_m \le t \le t_{m,e})$ is found as

$$\Delta N(\chi, z, t_m \le t \le t_{m,e}) = \Delta N_\infty\left\{1 - Se^{-\beta(t - t_m)}\right\}, \tag{14}$$

where,

$$S = \frac{4}{\beta t_m} + \frac{12}{\beta^2 t_m^2} - \frac{24}{\beta^3 t_m^3} + \frac{24}{\beta^4 t_m^4}(1 - e^{-\beta t_m}). \tag{15}$$

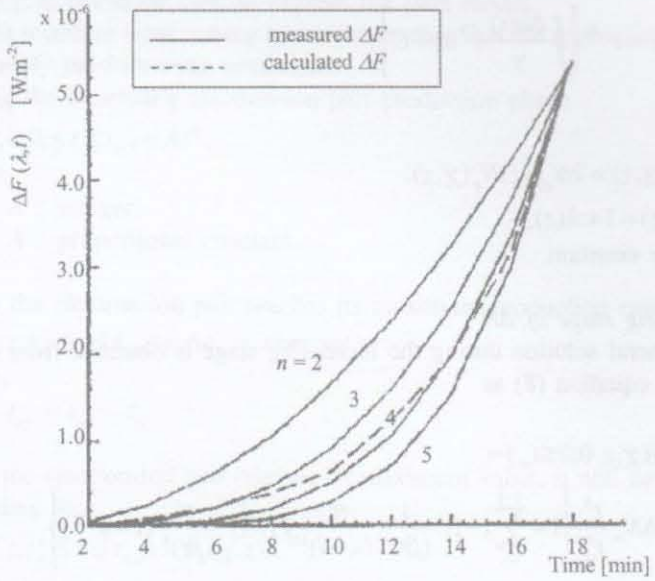


FIGURE 2. Determination of integer $n$

*Decreasing stage of $\Delta N$*

$\Delta N$ during the decreasing stage is obtained from equations (7) and (8). Equation (14) is also used when $\Delta N(t_{m,e})$ at the maximum stage is equal to $\Delta N(t_{m,e})$ at the decreasing stage. $\Delta N(\chi, z, t_{m,e} \le t \le t_e)$ is then found to be

$$\Delta N(\chi, z, t_{m,e} \le t \le t_e) =$$

$$\begin{Bmatrix} \Delta N_\infty \left[ \dfrac{\beta}{(\beta - B)} e^{-\beta(t-t_{m,e})} - \left\{ \dfrac{B}{(\beta - B)} + S e^{-\beta\tau_m} \right\} e^{-\beta(t-t_{m,e})} \right], \beta \neq B \\ \Delta N_\infty \left\{ 1 + \beta(t - t_{m,e}) - S e^{-\beta\tau_m} \right\} e^{-\beta(t-t_{m,e})}, \beta = B \end{Bmatrix}. \quad (16)$$

$B$ is obtained by setting

$$\Delta q(t_{m,e} + t_d) = b \Delta q(t_{me}), \quad (17)$$

where,

$b$ : proportional constant,

during the decreasing stage. From eqs. (17) and (8), $B$ is expressed by,

$$B = -\frac{1}{t_d} \ln b. \quad (18)$$

## TIME LAG AND RESPONSE RATE

$\Delta N$ is derived using the above flare model to get the time lag as shown in Figure 1. Time lag is one of the most important factor to evaluate the response of $\Delta N$ to $\Delta F$. The time lag, $t_{l,m}$ is obtained from the difference of

time of $\Delta N$ at maximum stage, $t_{\Delta Nm}$ with the time of $\Delta F$, $t_m$ during the increasing stage where,

$$t_{l,m} = t_{\Delta Nm} - t_m. \tag{19}$$

From eqs. (16), (19) and by replacing $t_m = t_{m,e} - \tau_m$, the time lag is given by,

$$t_{l,m} = \begin{Bmatrix} \dfrac{1}{(\beta - B)} \ln\left\{1 + \dfrac{(\beta - B)}{B} Se^{-\beta\tau_m}\right\} + \tau_m, \beta \neq B \\ \dfrac{1}{\beta} Se^{-\beta\tau_m} + \tau_m, \beta = B \end{Bmatrix}. \tag{20}$$

The time lag can also be expressed by a response rate, $R$, which indicates that the best response is 1 when $t_{l,m} = 0$. $R$ is expressed as,

$$R(\chi, z) = \frac{1}{\left(t_{l,m}(\chi, z) + 1\right)} \min^{-1}. \tag{21}$$

In most conditions, $t_{l,m} \geq 0$, which defines the range of $R$ as $0 < R(\chi, z) \leq 1$. This is an inverse expression of $t_{l,m}$.

## GOES-7 DATA

The GOES -7 data taken was reported in Abdullah and Zain (2000). Since this data is useful to obtain the time lag from observed $\Delta F$, to be compared with the theoretical time lag obtained from flare model, the data is presented again in this paper.

The SSX-ray data is time variation of the SSX-ray flux intensities with short and long wavelength ranges of 0.05~0.4 nm and 0.1~0.8 nm, respectively, which were observed by the X-ray detector on-board the Geostationary Operational Environmental Satellite (GOES). Two types of flares, the saw-tooth type (SWT), which has more than one maximum before its recovery to the quiet state and the smooth type (SOT), which has only one maximum, were selected from the SSX-ray intensity. The occupation of these two events,

SWT : 1988.11.13,20:00~14,05:07 UT, ($\tau_f$ = 547 min) and
SOT : 1989.7.9,00:00~9,10:07 UT, ($\tau_f$ = 607 min)

were selected from the stage of the increasing period in 22nd solar cycle (Solar-Geophysical Data 1988, 1990).

In the study of solar flares, the most important physical quantity is not the flux intensities themselves, but their increment from the quiet value. $\Delta F$ is essential in order to explain the magnitude of SIDs which can be taken from SSX-ray with time variations, $F(t)$. The start time of the SSX-ray was taken at in order to avoid a non-causal state of $\Delta F(t) < 0$. From the selected events, a time interval of one minute was chosen due to quite large flare

times (500~600 min). For the general theory described before, the parameters adopted in this paper are as follows,

1. Altitude $z$ = 40~150 km, $\Delta z$ = 10 km.
2. Zenith angle $\chi$ = 0, 60, 80 and 85°.
3. The two adjacent wavelength ranges are $0.05 \leq \lambda$ [nm] $< 0.1$ and $0.1 \leq \lambda$ [nm] $\leq 0.8$.
4. $Nq(\chi,z)$, $\lambda(z)$, $\alpha_{eff}$ $(z)$ and $Y(\chi,z,\lambda)$ were adopted from Sakagami's calculated data (Ohshio et al. 1966 ).

## RESULTS AND DISCUSSIONS

### COMPARISON OF TIME LAG BETWEEN OBSERVED AND FLARE MODEL

The time lag is one of the physical quantities used to show the best response of $\Delta N$ to $\Delta F$. It can be obtained using equation (20) as ${}_{th}t_{l,m}$. This value is compared with the time lag obtained from observations of $\Delta F$ as ${}_{ob}t_{l,m}$ which has been calculated previously (Abdullah & Zain 1999). Three representative events, $E_s1$, $E_i1$, and $E_i4$ of $\Delta F$ ($\lambda$ = 0.05 ~ 0.4nm,$t$) have been selected to calculate ${}_{th}t_{l,m}$. Subscript $s$ (smooth) is to show that the data selected is referred to some characteristic time of SOT and subscript $i$ (independent) means that the data selected is referred to some characteristic time of SWT. Details of the events are shown in Table 1 and Figure 3.

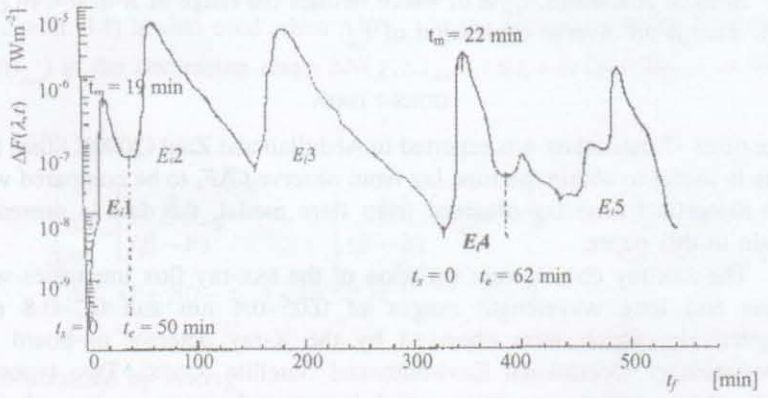


FIGURE 3. Representative events, $E_i1$, and $E_i4$

TABLE 1. Selected events from observed

| Time \ flare events | | $E_s1$ | $E_i1$ | $E_i4$ |
|---|---|---|---|---|
| Starting time | $t_s$ (UT) | 1989.07.00, 00:00 | 1988.11.13, 20:00 | 1988.11.14, 01:28 |
| | $t_{f,s}$ (min) | 0 | 0 | 0 |
| Ending time | $t_e$ (UT) | 1989.07.09, 10:00 | 1988.11.13, 20:30 | 1988.11.14, 02:30 |
| | $t_{f,e}$ (min) | 607 | 50 | 62 |
| Maximum time | $t_{f,m}$ (min) | 79 | 19 | 22 |

From equation (20), ${}_{th}t_{l,m}$ depends on $B$ of equation (18) and $\beta$ of equation (9). By substituting $b$ = 10 from observed data,

$$B = -\frac{1}{t_d}\ln b = \frac{2.3026}{t_d}, \tag{22}$$

where $t_d$ is obtained from the three events. $\beta$ is chosen at $\chi = 0°$ and $z = 100$ km due to a good response of $\Delta N$ to $\Delta F$. Table 2 shows the physical quantities used to calculate the ${}_{th}t_{l,m}$.

TABLE 2. Physical quantities of $\Delta F$

| Physical quantities / flare events | $E_s1$ | $E_i1$ | $E_i4$ |
|---|---|---|---|
| $\tau_m = t_{m,e} - t_m$ [s] | 0 | 0 | 0 |
| B [$s^{-1}$] | $1.83\times10^{-3}$ | $2.40\times10^{-3}$ | $5.73\times10^{-4}$ |
| $\beta(\chi = 0°, z = 100$ km) | $1.19\times10^{-1}$ | $1.19\times10^{-1}$ | $1.19\times10^{-1}$ |
| $S$ | $7.1\times10^{-3}$ | $2.9\times10^{-2}$ | $2.5\times10^{-2}$ |

Table 2 shows that $\beta >> B$ and $\tau_m = 0$ at all events. Substituting these conditions in equation (20) will result in

$${}_{th}t_{l,m} = \frac{1}{(\beta - B)}\ln\left\{1 + \frac{(\beta - B)}{B}S\right\}. \tag{23}$$

The time lag at $\chi = 0$, 60, 80 and 85° and $z = 0$, 60, 80 and 85° has been calculated for both ${}_{th}t_{l,m}$ and compared with ${}_{ob}t_{l,m}$. This is shown representatively in Figures 4(a) and 4(b) for event $E_i1$. From the results, we can conclude that for height variations,

1) At $z = 60$ km, ${}_{th}t_{l,m}$ and ${}_{ob}t_{l,m}$ increase slowly with increasing $\chi$ and at $z = 80$ and 100 km, it increases rapidly with increasing $\chi$ (Fig. 4(a)). Furthermore, it shows a continuously increasing function.
2) At $\chi = 0°$, ${}_{th}t_{l,m}$ and ${}_{ob}t_{l,m}$ show a continuously increasing function and at $\chi = 60$, 80 and 85°, it does not show a continuously increasing function due to the peak at $z = 80$ km (Fig. 4(b)). Both observed and theoretical values show that $t_{l,m}$ ($z = 100$ km) < $t_{l,m}$ ($z = 60$ km) < $t_{l,m}$ ($z = 80$ km).

The relationship between both time lags and $\Delta F_m(\lambda_l{\sim}\lambda_u, t)$ in most cases can be summarized as follows,

1) $t_{l,m}$ ($\chi$,z = 60 km) simply follows $\Delta F(\lambda,t)$.
2) $t_{l,m}$ ($\chi$,z = 80 km) also follows $\Delta F(\lambda,t)$ in most cases.
3) $t_{l,m}$ ($\chi$,z = 100 km) follows $\Delta F(\lambda,t)$ well for ≤ 2 min.

$t_{l,m}$ ($\chi$,z = 80 km) is larger than $t_{l,m}$ ($\chi$,z = 80 & 100 km) showing a poor response of $\Delta N$ to $\Delta F$. The results show that the theoretical and observed values correlate fairly well.

The time lag which can also be expressed by the response rate, $R$ (see Equation (21)), can be described as follows,

1) when z is fixed, $\chi$ increases with decreasing $R$ showing a continuously decreasing function,

2) when $\chi$ is fixed, $R(z = 100 \text{ km}) > R(z = 60 \text{ km}) > R(z = 80 \text{ km})$ which does not show a continuous function.

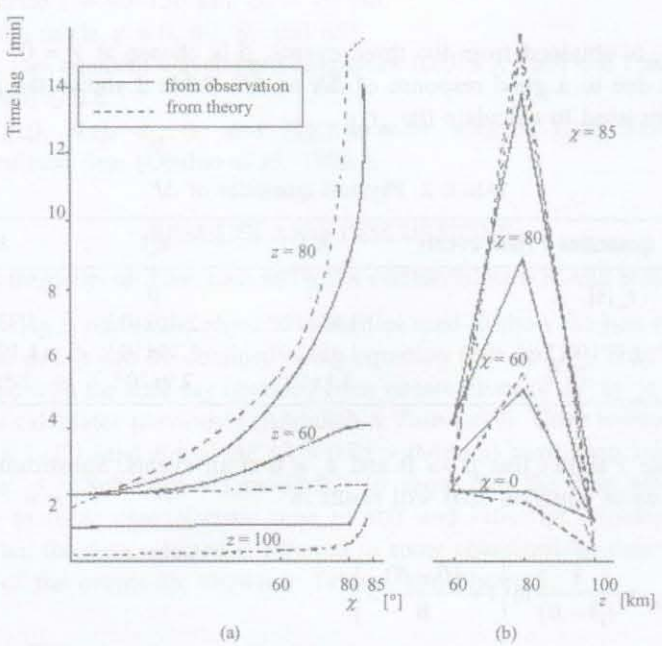


FIGURE 4. Time lag

DETERMINATION FACTOR OF RESPONSE RATE AND PHYSICAL QUANTITIES CONSTITUTING TIME LAG

The validity and significance of physical quantities constituting the time lag and response rate, which do not appear on observed data, can be identified and recognized. The physical quantities to be investigated from equation (20) are $\beta$, $S$, and $\tau_m$.

I. S is examined using equation (15). For values of $\beta(\chi = 0 \sim 85°, z = 60 \sim 100 \text{ km}) \sim 10^{-4} \sim 10^{-1}$ [s$^{-1}$], and $t_m \sim 10^3$, $\beta t_m$ will be $\sim 10^{-1} \sim 10^2$. For the following conditions,
   i) when $\beta t_m \leq 1$, $0 < 1 - e^{-\beta t_m} < 1$, as well as $1 < (\beta t_m)^{-1} << (\beta t_m)^{-4}$. Furthermore, the fourth term of the right side of equation (15) will result in $S \sim -10^1 (\beta t_m)^{-4}$ where $|S| >> 1$.
   ii) when, $\beta t_m > 1$, $1 - e^{-\beta t_m} \sim 1$, as well as $(\beta t_m)^{-1} >> (\beta t_m)^{-4} > 0$. Furthermore, the first term of the right side of equation (15) will result in $S \sim 4(\beta t_m)^{-1} < 1$.

II. The time lag is identified based on the above conditions using equation (20) when $\beta \neq B$.
   i) Using condition I. i) above, and substituting $\tau_m = 0 \sim 600$ [s], will get $\beta t_m \approx 0 \sim 6 \times 10^{-2}$ and $e^{-\beta \tau_m} = 0 \sim 1 < 1$. Furthermore $|(\beta - B)/B| = |\beta/B - 1| \leq 1$ and $S < 1$ are necessary to establish $|\{(\beta - B)/B\} S e^{-\beta \tau_m}| < 1$. Since this value is a function of natural log and $\leq 0 \sim 1$, it will not give a very small negative value. The necessity of $\tau_m$ is largely dependent on whether $\beta$ is bigger or smaller than $B$,

and whether the function of *ln* is bigger or smaller than 0. Furthermore, if $\beta$ is bigger than $B$, and the function of *ln* is bigger than *0* or $\beta$ is smaller than $B$, and the function of *ln* is smaller than 0, it is preferable that $\tau m \geq 0$. If $\beta$ is bigger than $B$, and the function of *ln* is smaller than 0 or $\beta$ is smaller than $B$, and the function of *ln* is bigger than 0, then it will result |the first term| < $\tau_m$ where this will ensure that $\tau_m > 0$.

ii) Using condition I. ii) above for the same $\tau_m$ will result in $\beta\ \tau_m \approx 0 \sim 6 \times 10^{-1}$, $e^{-\beta\tau_m} = 0 \sim 1 \leq 1$ and will satisfy S<1. These values determine that $\beta > B$. The second factor of equation (20) is largely dependent on $\beta$ / $B$ where $\beta$ is bigger with smaller B. However, since this value is a function of *ln*, whatever bigger value of $\beta$ will not give too big a positive value for the second factor. Therefore, equation (20) is dependent on $1/\beta$ and $\tau_m$. If $\beta$ is small, the determination factor is $\beta$ and $\tau_m$ and if $\beta$ is big, the determination factor is $\tau_m$ only. If the determination factor is b, time lag is small according to big value of $\beta$. Furthermore, the response rate is also big which shows a good response of $\Delta N$ to $\Delta F$.

III. The time lag is identified based on the above conditions using equation (20) when $\beta = B$.
For the same condition as II. i), this will result in $S < 0$ where $|S| >> 1$. However, in order to satisfy $t_{l,m} \geq 0$, it is necessary that the second term should be bigger than the first term of equation (20). If $\beta$ is small for smaller $S < 0$, the time lag will be small and give a good response to $\Delta F$ and vice versa.

Through conditions II. and III. above, the condition where $\beta \neq B$ is more acceptable than $\beta = B$ in general. This is also shown in Table 2. Since, $\beta >> B$ and $\tau_m = 0$, the most suitable condition is II. ii). Thus, equation (23) can be simplified as

$$_{th}t_{l,m} = \frac{1}{\beta}\ln\left\{1+\frac{\beta}{B}S\right\}. \tag{24}$$

The above equation is dependent on $1/\beta$, and $(\beta/B)S$. However, the rapid changes of a function of *ln* do not really affect the first term of the equation. So we can conclude that $\beta$ is an important determination factor of time lag. Finally, we can conclude that time lag is inversely proportional to $\beta$, which shows a good response.

## EXPLANATION ON $\beta$ AS A DETERMINATION FACTOR OF RESPONSE RATE

*Variation of* $\beta$

The variation of $\beta$ is investigated at $\chi = 0$, 60, 80, and 85° using equation (9) to compare with the response rate. The results are shown in Table 3. In general, $\beta$ increases with smaller $\chi$. With independent $\chi$, it is understood that $\beta(\chi, z = 100\ \text{km}) > \beta(\chi, z = 60\ \text{km}) > \beta(\chi = 60, 80, 85°, z = 80\ \text{km})$. This means that $\beta$ shows a decreasing function with respect to $\chi$ and not a decreasing function with respect to z due to a minimum value at which

TABLE 3. Variation of $\beta$

| z(km)/ | 0 | 60 | 80 | 85 |
|---|---|---|---|---|
| 100 | $1.19\text{x}10^{-1}$ | $5.89\text{x}10^{-2}$ | $3.42\text{x}10^{-2}$ | $1.28\text{x}10^{-2}$ |
| 80 | $8.62\text{x}10^{-3}$ | $1.72\text{x}10^{-3}$ | $2.24\text{x}10^{-4}$ | $2.07\text{x}10^{-4}$ |
| 60 | $6.46\text{x}10^{-3}$ | $6.12\text{x}10^{-3}$ | $5.94\text{x}10^{-3}$ | $5.94\text{x}10^{-3}$ |

shows poor response of to $z = 80$ km. This result is significant in order to explain the variation of the response rate at selected value as calculated above.

*Height distribution of* $\beta$

To see variation of $\beta$ in detail, $\chi$ at 0, 30, 50, 60, 70, 80, 85 and 90° are plotted at every km of altitude ranging from 40 km to 150 km as shown in Figure 5. It clearly showssss a cusp, which indicates a decreasing function with respect to $\chi$ and not a decreasing function with respect to z due to minimum value from $\beta_{min}(\chi = 0°, z = 72$ km) towards $\beta_{min}(\chi = 90°, z = 78$ km). Even though it was previously concluded that $z = 80$ km shows a poor response of $\Delta N$ to $\Delta F$, it is much better to consider heights at $z = 72 \sim 78$ km since these heights are observed to be more affected. At $z \leq 60$ km, $\beta$ has the same value at all $\chi$ and at $z > 60$ km, $\beta$ increases depending on different values of $\chi$. However, at $z > 100$ km, $\beta$ does not expand well where at $\chi = 0 \sim 70°$, $\beta$ shrinks depending on different $\chi$. This characteristic shows that $R(\chi,z = 100$ km) or $t_{1/2}(\chi,z = 100$ km) clearly exhibits the differences of $\chi$, but not clear at $z = 80$ km and not even shown at $z = 60$ km (see also Figure 4).

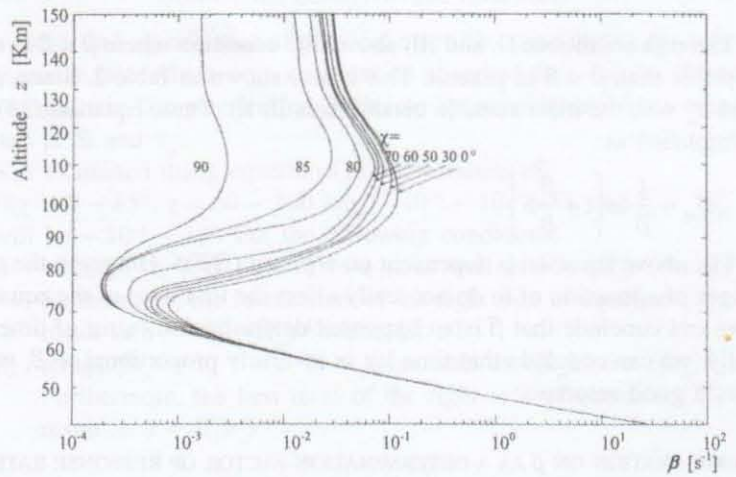


FIGURE 5. Height distribution of $\beta$

## CONCLUSIONS

From the analysis of the flare model, we can conclude that the variations of $\Delta N(\chi,z,t)$ follow in-step the change in $\Delta F(\lambda_l \sim \lambda_u,t)$. It is mostly dependent on fundamental physical quantities, $\beta(\chi,z)$ by evaluation of the response rate. This shows that by using flare model, the corresponding values of

$N(\chi,z,t)$ or $\Delta N(\chi,z,t)$ can be directly computed and the response of observed values of $\Delta F(\lambda_l \sim \lambda_u,t)$ can be compared to GOES-7. By knowing the determination factor, the flare model can also predict the $\Delta N(\chi,z,t)$ on a long-term basis for predicted solar activities. The processed data will exceedingly be useful for ionospheric physics and the study of ionospheric radio propagation.

ACKNOWLEDGEMENT

The authors would like to thank Professor Ohshio at Okinawa Observatory, Japan for the valuable discussion and providing the data for this study.

SYMBOLS

| | |
|---|---|
| $\alpha_{eff}$ | effective recombination coefficients |
| $\beta$ | substituted expression of $2\alpha_{eff}(z)N_q(\chi,z)$ |
| $\Delta$ | difference of a physical quantity during solar X-ray flare from that in quiet state |
| $\lambda$ | wavelength |
| $\chi$ | solar zenith angle |
| $B$ | decreasing coefficient of $\Delta q$ |
| $F$ | solar x-ray flux intensity |
| $N$ | electron density |
| $q$ | production rate of electron-ion pairs |
| $q(suffix)$ | quite state |
| $R$ | response rate |
| $t$ | time |
| $t(suffix)$ | theoretical calculated |
| $Y$ | local photoionization efficiency |
| $z$ | altitude from the earth surface |

REFERENCE

Abdullah, M. & Zain, A.F.M. 2000. Determination of D-region electron densities, from GOES-X-ray detector measurements. *J. Institution of Engineers* 61(3): 67-80.

Bentley, R. D. & Phillips, A. T. 2005. Yohkoh Analysis Guide. (on-line) http://umbra.gsfc.nasa.gov/sdac.html#YAG (11 July 2005).

Dellinger, J. H. 1937. Sudden Inospheric Disturbances. *Terr. Mag. And Atmos. Elec.* 42: 49-53.

Holman, G. & Benedict, S. 2003. Solar flare theory. (on-line) http://hesperia.gsfc.nasa.gov/sftheory/ (11 July 2005).

Millward, G. H., Moffett, R. J., Balmforth, H. F., & Rodger, A. S. 1999. Modeling the ionospheric effects of ion and electron precipitation in the cusp. *J. Geophys. Res.* 104(A11): 24.

Ohshio, M. 1978. Ionospheric D-region disturbances caused by solar X-ray flares. Radio Res Lab. Report, Tokyo.

Ohshio, M., Maeda, R. & Sakagami, H. 1966. Height distribution of local photoionization efficiency. *J. Radio Research Lab.* 13(70): 245-577.

Rishbeth, H. 1969. *Introduction to ionospheric physics.* International Geophysics Series. New York: Academic Press Inc.

Solar-Geophysical Data Comprehensive Report. 1988 & 1990. Nos. 545 and 537, NOAA: USA.

Mardina Abdullah
Department of Electrical, Electronic and Systems Engineering
Faculty of Engineering
Universiti Kebangsaan Malaysia
43600 UKM Bangi, Selangor D.E.
E mail: mardina@eng.ukm.my

Ahmad Faizal Mohd. Zain
Faculty of Graduate Studies
Kolej Universiti Teknologi Tun Hussein Onn
Batu Pahat, Johor, D.T.
E mail: drfaizal@ieee.org